



HAL
open science

Malonate Complexes at γ -Alumina Surface Determined by a Multitechnique Characterization Approach and a Surface Complex Model

Teddy Roy, Manuel Corral-Valero, Thibaut Corre, Olivier Delpoux, Gerhard Pirngruber, Grégory Lefèvre

► **To cite this version:**

Teddy Roy, Manuel Corral-Valero, Thibaut Corre, Olivier Delpoux, Gerhard Pirngruber, et al.. Malonate Complexes at γ -Alumina Surface Determined by a Multitechnique Characterization Approach and a Surface Complex Model. *Colloids and Surfaces A: Physicochemical and Engineering Aspects*, 2022, 634, pp.127923. 10.1016/j.colsurfa.2021.127923 . hal-03602564

HAL Id: hal-03602564

<https://ifp.hal.science/hal-03602564>

Submitted on 9 Mar 2022

HAL is a multi-disciplinary open access archive for the deposit and dissemination of scientific research documents, whether they are published or not. The documents may come from teaching and research institutions in France or abroad, or from public or private research centers.

L'archive ouverte pluridisciplinaire **HAL**, est destinée au dépôt et à la diffusion de documents scientifiques de niveau recherche, publiés ou non, émanant des établissements d'enseignement et de recherche français ou étrangers, des laboratoires publics ou privés.

1 Malonate complexes at γ -alumina surface determined by a multi- 2 technique characterization approach and a surface complex model

3 Teddy Roy^{a,b}, Manuel Corral Valero^a, Thibaut Corre^a, Olivier Delpoux^a, Gerhard Pirngruber^a, Grégory
4 Lefèvre^{b*}

5 ^a IFP Energies nouvelles, Rond-point de l'échangeur de Solaize, 69360 Solaize, France

6 ^b Chimie ParisTech, PSL Research University, CNRS, Institut de Recherche de Chimie Paris (IRCP), F-75005
7 Paris, France

8 *Corresponding author e-mail and phone number:

9 gregory.lefevre@chimieparistech.psl.eu / +33 (0)1 85 78 42 68

10

11 Abstract

12 γ -Al₂O₃ is a transition alumina oxide used in many different applications. Its surface chemistry
13 seems to be a key factor in the preparation of heterogeneous catalyst where γ -Al₂O₃ is used as a
14 support. The modification and description of its surface are necessary to understand the role of the
15 support on the catalyst preparation and on its performance. In this work, the modification of the
16 surface is performed with a carboxylic diacid, malonic acid, which specifically adsorbs at the γ -Al₂O₃
17 surface and modifies the surface chemistry (surface sites density and global surface charge). The impact
18 of the impregnation pH, malonic acid content, and drying are studied. By using a multi-technique
19 approach, both the solid/liquid interface and the dried surface were characterized. The infrared
20 spectroscopic information coupled with zetametry measurements indicate the formation of an inner
21 sphere complex adsorbed via both side-on ester linkage and bridging bidentate mode involving the two
22 carboxylic groups. A surface complexation model was built to support the experimental results and
23 obtain complementary information. It underlines the different reactivity of the γ -Al₂O₃ facets and of the
24 surface sites responsible for the adsorption. The whole (100) facet is involved in the adsorption while
25 only the μ_1 -Al_{VI}-OH and μ_1 -Al_{IV}-OH sites of the (110) facet participate in the malonic acid adsorption. The
26 model also confirms the consumption of 3 to 4 surface hydroxyls per adsorbed molecule, in accordance
27 with ester linkage and bridging bidentate structure. This molecular level description of the surface
28 chemistry is of interest in different environmental fields such as wastewater treatment and pollutant
29 removal. In the catalysis field, the detailed surface chemistry will be very useful to understand the
30 impact of this modified support on the catalytic performance.

31 Keywords

32 Malonic acid, gamma-alumina, surface complexation models, solid/solution interface, PhreeqC

33 Introduction

34 The interaction between organics and metal (hydr)oxides surface is of interest in many application fields
35 such as environmental chemistry (pollutants removal through adsorption¹), chemical waste
36 treatments², and catalysis (e.g. hydrotreating catalyst^{3,4}). For this latter application, the strong
37 interaction between the active phase of the catalyst and the support is often mentioned to play a key
38 role on the final catalytic activity⁵⁻⁸. By adding an organic additive during the catalyst preparation, this
39 active phase-support interaction can be tuned, with a strong impact on the performance. Thus, the
40 identification of complexes adsorption on metal (hydr)oxides surface at the solid/liquid interface at a
41 molecular level is a real challenge both from a fundamental and from an industrial point of view.

42 The interaction of organic acids with γ -Al₂O₃ is of particular interest for catalyst preparation since this
43 support is widely used in heterogeneous catalysis, for example in case of hydrotreating and Fischer-
44 Tropsch catalysts^{9,10}. Indeed, carboxylic acids used as an additive during the catalyst preparation can
45 positively impact the catalytic performance¹¹. This increased activity could be explained by a delayed
46 sulphidation³ (activation stage of the catalyst), a better dispersion or a weakened interaction with the
47 support due to metal precursors' complexation¹² by the additive. Another role the additive could play, is
48 the modification of the surface chemistry of the support which will in turn impact the active phase
49 support interaction. The ability of carboxylic acid to strongly modify the alumina surface by specific
50 bonding¹³⁻¹⁵ could be a useful property in order to understand the role of the support during catalyst
51 preparation. As an example, one of the most studied carboxylic acid additive, citric acid¹⁶⁻¹⁸, has proved
52 to increase the catalytic activity when pre-impregnated onto the support¹⁹. However, intrinsic
53 properties of citric acid such as its tendency to favour metals reduction^{20,21} or complexing properties
54 with both, the promoter and active phase precursor depending on the solution pH⁴ added to its possible
55 degradation²² make it difficult to rationalize the role of the support. In that sense, malonic acid, rarely
56 studied in the hydrotreatment field (sometimes evocated as an additive²³ or rejuvenation agent for
57 spent catalyst²⁴⁻²⁶), is a valuable candidate as it adsorbs specifically at the γ -Al₂O₃ surface^{2,13,27} and does
58 not interact with metallic precursors or degrade at the surface. In this work, malonic acid has been
59 chosen to tune the surface chemistry of catalyst support.

60 Consequently, the description at a molecular level of the γ -Al₂O₃ surface modified by malonic acid
61 represents a first important step in the characterization of the role of the support for further
62 heterogeneous catalysts preparation and performance studies. This system has already been studied
63 using *in situ* attenuated total reflection-infrared spectroscopy, ATR-FT-IR. Using the latter technique,
64 Dobson *et al.*¹³ have proposed that adsorption takes place through ester linkage via the two carboxylic
65 groups. However, in a recent study on the interaction of europium (III) with γ -Al₂O₃ in the presence of
66 malonic acid, Patel *et al.*², based on ATR-FT-IR and Time Resolved Fluorescence spectroscopic data,
67 proposed the formation of a bidentate mononuclear complex as well as a protonated bidentate species,
68 involving two and one carboxylic groups, respectively. This shows that the geometry of the complex is
69 still not clearly defined. Moreover, these research works focus on the solid/liquid interface while a
70 further drying stage is applied during the catalyst preparation and might impact the geometry of the
71 complex. Finally, these previous studies are focused on the geometry of the adsorbate, but the
72 adsorption sites involved in the malonic complex formation at the γ -Al₂O₃ surface were not

73 investigated. These two features (evolution during drying and reactive sites) are essential in the
74 understanding of the role of the support in catalysis and are addressed in this study.

75 In the present work, the modification of the γ -Al₂O₃ surface chemistry induced by the impregnation of
76 malonic acid at different contents (from 0.2 to 0.9 malonic acid/nm²) is described. The adsorption at the
77 solid/liquid interface was quantified by adsorption isotherms and was probed by *in situ* ATR-FT-IR and
78 zetametry techniques. The impact of a drying stage on the geometry of the surface complexes is also
79 discussed based on infrared spectroscopy characterizations. Finally, by using the information derived
80 from the characterizations, a surface complexation model has been built based on a DFT description of
81 the hydrated alumina surface²⁸⁻³¹ and the MUSIC model³². This simulation is an approach we have
82 developed to support the experimental data and obtain complementary information on the complex
83 geometry, the reactivity of γ -Al₂O₃ faces and of the surface sites involved in the adsorption process.

84 Experimental/method Section

85 Adsorption isotherm/ ionic chromatography

86 The support was prepared by peptization of AlOOH boehmite Pural SB3 (purchased from Sasol) with
87 concentrated nitric acid, molding by extrusion and calcination in air at 540°C for 4 hours. These γ -Al₂O₃
88 extrudates were crushed to obtain particles between 400 and 800 μ m in order to avoid diffusion
89 limitations. The support had a surface area of 209 m² g⁻¹ determined by nitrogen physisorption and a
90 pore volume of 0.88 cm³ g⁻¹.

91 The adsorption isotherm of malonic acid was measured under atmospheric conditions by contacting γ -
92 Al₂O₃ with solutions of different initial concentrations at constant temperature, 25°C and at pH 4. 2
93 grams of solid were introduced in a batch reactor containing a volume of solution equal to ten times the
94 pore volume, i.e. 17.6 mL, at a specific concentration of malonic acid and pH. Then, it was stirred for 3
95 hours to assure the equilibrium as it is usually reached in less than an hour for the system carboxylic
96 acid/alumina^{2,33}. During the experiment, the pH was checked every 30 minutes and maintain at 4 by the
97 addition of a small volume of HNO₃ (10⁻¹ mol L⁻¹, Fischer Scientific). The initial solution concentration of
98 malonic acid (99%, VWR reagents) ranged from 5.10⁻³ to 2.5.10⁻¹ mol L⁻¹ and its pH was adjusted by a
99 solution of NaOH (0.1 mol L⁻¹, VWR reagents). It is worth noted that the ionic strength was not control
100 by the addition of an electrolyte for all solid/solution experiments. Indeed, the main purpose of the γ -
101 Al₂O₃ surface modification is to prepare catalyst's support. However, addition of foreign ions, such as
102 Na⁺, represents a poison for the catalyst and thus their addition has been excluded.

103 Both initial and final concentration of malonic acid were measured by ionic chromatography. This
104 quantification was performed on an ECO IC (Metrohm) using a Shodex IC-SI-354D analytical column
105 (150 mm length x 4 mm I.D.) at 45°C with isocratic 3.6 mM Na₂CO₃ eluent at a flow rate of 1.2 mL min⁻¹.
106 The differences between the initial and the final concentration gives access to the malonic acid content
107 at the surface. After the adsorption isotherm and a filtration step, a drying of the solids (120°C, 6h) is
108 applied. Then, each solid is divided into two parts. The first part of the solid was used to perform the

109 zetametry measurements. For the second part, a washing step was performed with distilled water
110 (2x10mL) to measure the quantity of released malonic acid in solution by rinsing. The same
111 quantification procedure with ionic chromatography was used to determine the surface coverage.

112 **Sample preparation by incipient wetness impregnation (IWI)**

113 Several solids were prepared by incipient wetness impregnation³⁴ (IWI) in order to control the surface
114 coverage of malonic acid (0.2, 0.6 and 0.9 molecule/nm²) and further FT-IR characterizations. The
115 crushed extrudates used as supports are the same as those used for the adsorption isotherm. As a
116 starting reagent malonic acid was dissolved in water and the pH adjusted at 4 by NaOH (0.1 mol L⁻¹). The
117 impregnation solution concentration ranged from 7.5.10⁻² to 2.9.10⁻¹ mol L⁻¹ to reach the targeted
118 coverage. Another solid was impregnated to reach the value of the experimental monolayer (0.9
119 molecule/nm²) with a solution adjusted at pH 6.8 with NaOH. For each coverage, 5 grams of γ -Al₂O₃
120 were impregnated by 4.4 mL of the impregnation solution. The solid was placed under a saturated
121 water vapour atmosphere for 16 hours for an aging stage and then dried at 120°C for 6 hours.

122 **ATR-FT-IR in/ex situ**

123 The ATR-FT-IR spectra were collected in the range 4000-650 cm⁻¹ with a dry-air-purged Thermo
124 Scientific Nicolet IS50 FT-IR equipped with a MCT-B detector. Spectral resolution was 4 cm⁻¹ and spectra
125 were averaged from 256 scans. The crystal used was a single reflection diamond/ZnSe crystal with an
126 incidence angle of 45°C (Smart PIKE). In order to maximize the contact between the sample and the
127 crystal, the sample was crushed to powder before deposition on the crystal and then pressed onto the
128 crystal during the analysis. Data processing was carried out using OMNIC software. All spectra were
129 treated using the same procedure: atmospheric correction, advanced ATR correction and automatic
130 baseline correction between 900 and 18500 cm⁻¹.

131 The *in situ* ATR-FT-IR spectra were collected with the same spectrometer and recording parameters.
132 First, the horizontal diamond/ZnSe crystal was coated with 1 μ L of a γ -Al₂O₃ suspension (1 g L⁻¹) which
133 was dried under a flow of N₂. This procedure was repeated twice. A flow cell was clamped on the ATR
134 accessory. In order to stabilize the coating, distilled water adjusted at pH 4 with HNO₃ (1 M) was flushed
135 on the oxide film with a constant flow rate of 1 mL min⁻¹ using a peristaltic pump (Ismatec S.A.) at room
136 temperature. After 30 minutes, the stabilization of the coating was checked by the absence of
137 difference between two consecutive spectra, the background spectrum was then recorded and a
138 malonic solution (10⁻³ mol.L⁻¹) adjusted at pH between 9 and 4 by NaOH or HNO₃ (0.1 mol L⁻¹) was used
139 as the circulating solution.

140 **Transmission FT-IR Spectroscopy**

141 The FT-IR spectra were collected using a Vertex 70 spectrometer in the 4000-400 cm⁻¹ range. Spectral
142 resolution was 4 cm⁻¹ and spectra were averaged with 32 scans. The powdered samples of
143 approximately 20 mg were pressed into self-supporting pellets of 16 mm in diameter. The samples were
144 activated at 120°C under high vacuum (< 10⁻⁵ mbar). This condition allowed to prevent the degradation

145 of organic molecules but did not remove all the physisorbed water from the alumina surface. Data
146 processing was carried out using OMNIC and Origin software.

147 Zetametry measurements

148 The zeta potential measurements were performed using a Malvern Nano ZS Zetasizer. Zeta potentials
149 were calculated from measured electrophoretic velocity rates using the Smoluchowski equation. Before
150 the measurement, the dried solid was grounded in order to obtain powder and avoid the settling
151 problem. Thus, measurements were carried out using 100 mg of powdered samples suspended in 100
152 mL of aqueous solutions under stirring. The pH of the suspension was adjusted with 0.1 M HNO₃ and 0.1
153 M (or 0.01 M) NaOH solutions (prepared from VWR commercial solutions). The starting pH was adjusted
154 around 3. After a few minutes of equilibration, an aliquot was withdrawn and analyzed using the
155 Zetasizer. It was then poured back in the reactor. After adjusting the pH with NaOH, a new aliquot was
156 withdrawn when the pH value was stable. The protocol was repeated until pH reached a value of
157 approximately 10.

158 PHREEQC Modelling

159 PHREEQC2 speciation software was used to model the zetametry curve progression with increasing
160 malonic acid coverage. As in a previous study³⁵, the acido-basic equilibria at the alumina surface
161 determined by Corral Valero *et al.*³² have been used with basic Stern model as an electrostatic model
162 with a capacitance of 1.39 F/m² and ion pair formation constant (log K) of 0.096 for Na⁺ and 0.176 for Cl⁻
163 based on the parameters used by Mayordomo *et al.*³⁶

164 The zeta potential values cannot be calculated with accuracy due to the difficulty to locate the shear
165 plane, so its experimental value was compared to the value of the potential at the Stern plane (ψ_1), near
166 to the shear plane but located slightly closer in the diffuse layer³⁷. Nevertheless, Stern and shear plane
167 potentials coincide when their value is close to zero.

168 Since the adsorption of malonic acid was shown to be irreversible (after drying), the sorption
169 equilibrium was not implemented in the PHREEQC code. The protocol which was followed was to
170 replace a given fraction of hydroxyl sites by a surface adsorption complex, according to the
171 stoichiometry of the assumed adsorption reaction and the surface density of adsorbed malonate. For
172 the solution equilibria, the database Thermoddem v1.10 has been used, completed by the
173 deprotonation equilibria with malonic acid³⁸. An example of the PHREEQC code used for a malonic
174 content of 0.9 molecule/nm² is given in the supporting information (PHREEQC Script).

175

176

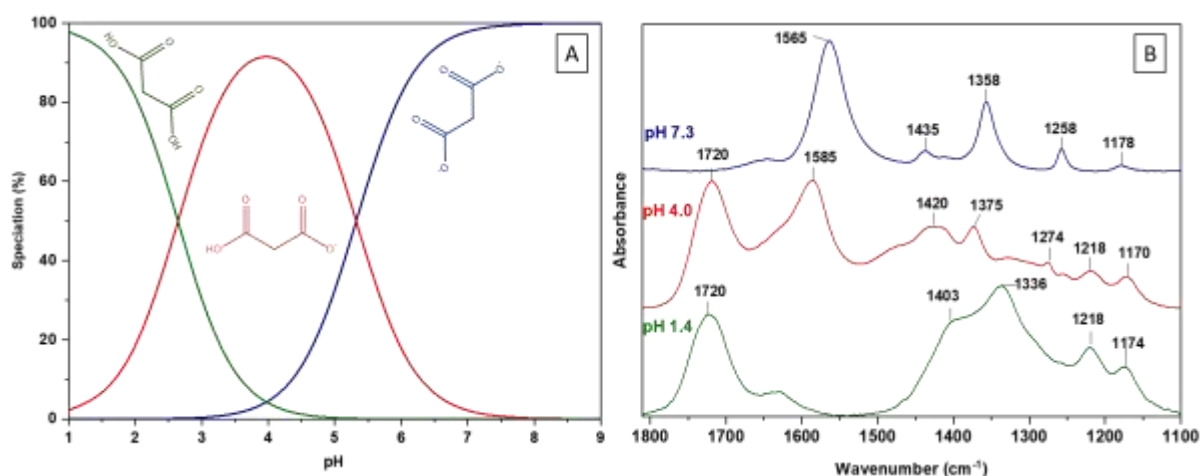
177

178 **Results/discussion**

179

180 **Solution speciation**

181 Malonic acid is a dicarboxylic acid with two protonation constants, leading to three possible species as a
 182 function of the pH. The pH chosen to perform the impregnation is thus of high importance. As shown in
 183 Figure 1.A, the diprotonated species (AH_2) dominates for the most acid solutions ($pH < 2.8$), the
 184 monoprotinated species (AH^-) for intermediary pH, between the two pK_a s ($2.8 < pH < 5.3$) and the
 185 dicarboxylate (A^{2-}) for the most basic solutions ($pH > 5.3$).



186

187 **Figure 1 : (A) Speciation diagram of malonic acid forms in solution calculated with PHREEQC (B) ATR-FT-IR spectra of malonic**
 188 **acid solution at $C = 10^{-1} \text{ mol L}^{-1}$ at pH 1.4, 4.0 and 7.3 in the $1800\text{-}1100 \text{ cm}^{-1}$ area**

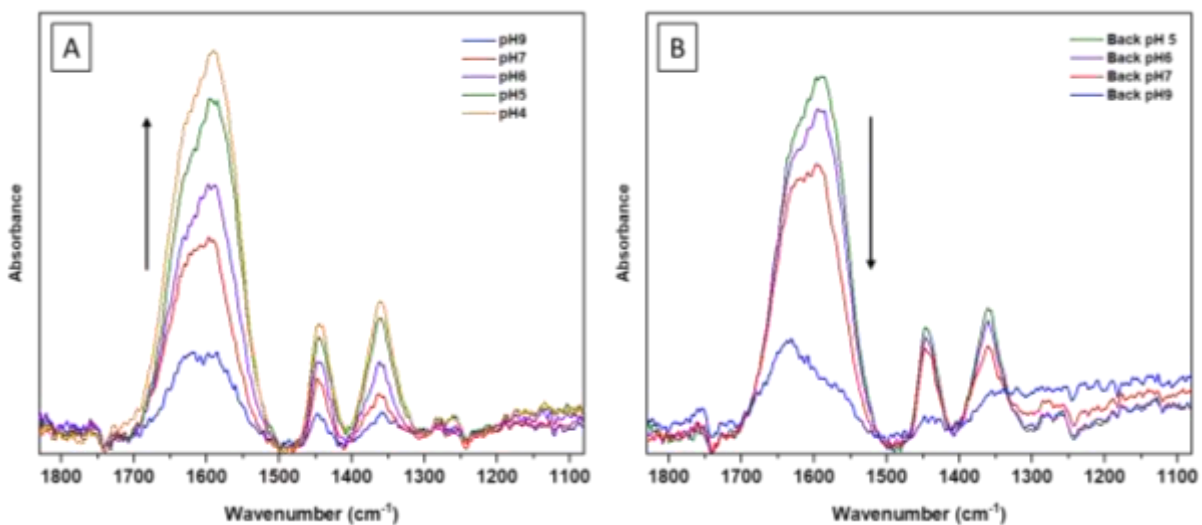
189 The infrared signature of the three species differs mainly because of their protonation degree (Figure
 190 1.B). The di- and monoprotinated acids have a $HO-C=O$ group in common giving rise to an intense band
 191 around 1720 cm^{-1} ($\nu_{C=O}$). Other strong infrared bands can be found in the $1590\text{-}1560 \text{ cm}^{-1}$ range and
 192 around $1375\text{-}1350 \text{ cm}^{-1}$, which corresponds respectively to the asymmetric and symmetric stretchings
 193 of carboxylate COO^- group present in both the deprotonated and partially deprotonated malonic acid.
 194 Between the spectra of the solution at pH 4 and the one at pH 7.3, a red shift is observed for both
 195 asymmetric and symmetric stretchings (1585 to 1565 cm^{-1} and 1375 to 1358 cm^{-1} , respectively). This is
 196 due to the complete deprotonation of the diacid. The last band of interest in this region is the one at
 197 1430 cm^{-1} assigned to the CH_2 bending mode. The spectrum recorded at pH 4 possesses characteristic
 198 band for both carboxylic and carboxylate groups. Less intense bands are observed at 1258 cm^{-1} ,
 199 attributed to a CH_2 bending mode, one at 1218 cm^{-1} , attributed to C-OH stretching and finally one at
 200 1170 cm^{-1} , which is attributed to CCH bending^{13,39}

201 The different spectral signatures observed in solution give a first indication on the way to differentiate
 202 the protonated and deprotonated forms of malonic acid before interacting with the $\gamma\text{-Al}_2\text{O}_3$ surface.
 203 Nevertheless the geometry of the molecule can drastically change once adsorbed at the surface⁴⁰, and
 204 the spectra of the adsorbates can be very different from any dissolved species.

205 In this article, the term “malonic acid” encompasses the three protonation states (diacid, anionic
 206 monoacid and dianion whose distribution is plotted in Figure 1) to simplify the writing. When it refers to
 207 the diacid molecule, it is specified in the text.

208 Solid/liquid interface characterization

209 The adsorption process of malonic acid has been followed by an *in situ* ATR-FT-IR experiment as a
 210 function of pH. The *in situ* experiment can track any change in the complex adsorption mode or
 211 geometry induced by a modification of the solution pH and can thus help to determine the adsorption
 212 mode of the complex formed at the alumina surface and the potential influence of the pH. The figure 2
 213 presents the evolution of the infrared signal when the pH is changed from 9 to 4 (Figure 2.A) and back
 214 from 5 to 9 (Figure 2.B).

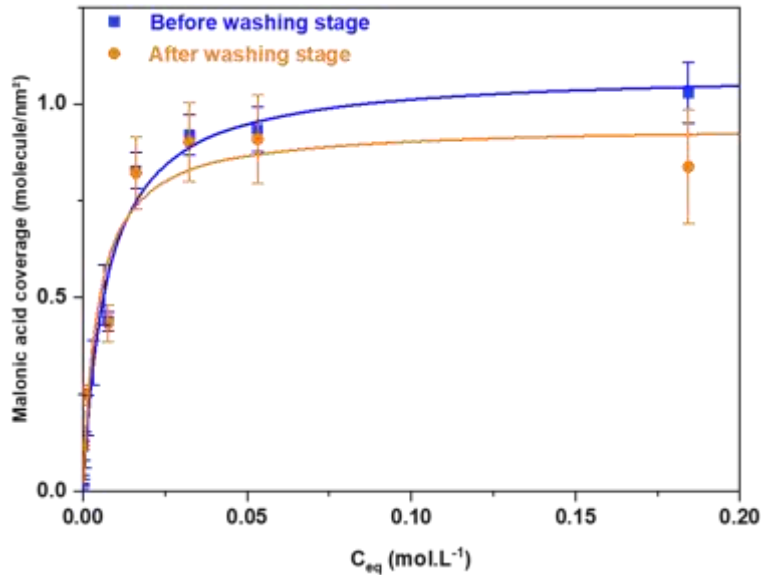


215
 216 **Figure 2 : *in situ* ATR-FT-IR spectra of the sorption of malonic acid from a solution at $C = 10^{-3} \text{ mol L}^{-1}$ as a function of pH. (A)**
 217 **from pH 9 to 4 and (B) from pH 4 to 9.6.**

218 The intensity of the signal evolves but the spectral signature remains unchanged on the whole pH range
 219 except for the return to pH 9 where the signal shape changes. This observation suggests the presence of
 220 a unique adsorption mode irrespective of the solution pH (at least in the range of $\text{pH} = 4$ to 7).
 221 Moreover, the spectra have the same spectral signature as the one recorded at even lower pH value
 222 ($\text{pH}=2$) found in the literature². This information confirms that the surface complex is insensitive to
 223 values lower than the first protonation constant ($\text{p}K_{a1}=2.8$). The evolution of the signal indicates a
 224 favoured adsorption of malonic acid at acidic pH since the intensity increases when the pH decreases
 225 (Figure 2.A). On the opposite, the signal decreases when the pH is increased (Figure 2.B), indicating a
 226 desorption process due to pH change when no drying stage is applied. The lowest pH value was limited
 227 to 4 in order to avoid the support's dissolution. However, a decreasing intensity would be expected at
 228 lower pH, as it is observed for malonic acid adsorption on anatase or lepidocrocite⁴¹.

229 In any case, *in situ* ATR-FT-IR, as expected⁴¹, proved that malonic acid adsorbs specifically on alumina.
 230 The geometry of the adsorbed complex at the solid/liquid interface (further discussed) does not depend

231 on the starting solution pH but the amount of adsorbate does, with an optimum pH in our study range
 232 around 4. Consequently, this pH value has been used to measure an adsorption isotherm. The Figure 3
 233 presents the adsorption isotherms before and after a washing stage determined by ionic
 234 chromatography.



235

236 **Figure 3 : Adsorption isotherms of malonic acid at the alumina surface performed at pH=4 and room temperature, 3h**
 237 **equilibrium impregnation. Estimated error : ± 5%**

238

239 The isotherm exhibits a plateau around 0.9 molecule/nm² after the washing stage which indicates the
 240 quantity required to form a malonic acid monolayer at the alumina surface. These isotherms also
 241 confirm a strong interaction of the malonic acid with the surface since it starts to adsorb at low
 242 concentration. The weak impact of the washing stage indicates that most of the malonic acid molecule
 243 is adsorbed specifically by forming an inner sphere complex and only a small amount would form an
 244 outer-sphere complex or be adsorbed electrostatically onto the surface.

245

$$246 \quad Q = \frac{Q_{max}K_L C_{eq}}{1 + K_L C_{eq}} \quad (\text{eq.1})$$

247

248 The Langmuir model has been used in order to fit the experimental data. It is represented by equation 1
 249 where Q is the equilibrium amount of adsorbed malonic (mol g⁻¹), C_{eq} is equilibrium concentration of
 250 malonic acid in solution (mol L⁻¹), Q_{max} (mol g⁻¹) is the maximum adsorption capacity and K_L the Langmuir
 251 constant. The fit was realized following a least squares procedure. Q_{max} was converted to N_{max} in
 252 molecule/nm² using the specific surface of the support (209 m² g⁻¹). The Langmuir constant gives an
 253 indication on the adsorption strength. The Langmuir isotherm parameters presented Table 1 are in the

254 same order of magnitude than other acids, such as acetic and propionic acid, adsorbed on α -alumina³³
 255 but the Q_{\max} for these monoacids (Table 1) is around 50% higher, probably due to the size of the
 256 molecule and steric hindrance. A stronger affinity, higher K_L (Table 1), could be explained by a chelation
 257 effect, since malonic acid has two carboxylic groups.

258

259 **Table 1 : Langmuir fitting parameters for the isotherms before and after washing stage compared to Langmuir parameters of**
 260 **acetic and propionic acid adsorption on α -Al₂O₃ from literature³³**

Isotherm	Q_{\max} (mol g ⁻¹)	K_L (L mol ⁻¹)	R ²	N_{\max} (molecule/nm ²)
Before washing	3.89x10 ⁻⁴	114	0.956	1.08
After washing	3.33x10 ⁻⁴	193	0.908	0.94
Acetic acid on α -Al ₂ O ₃	6.1x10 ⁻⁴	45	0.966	/
Propionic acid on α -Al ₂ O ₃	6.4x10 ⁻⁴	61.6	0.990	/

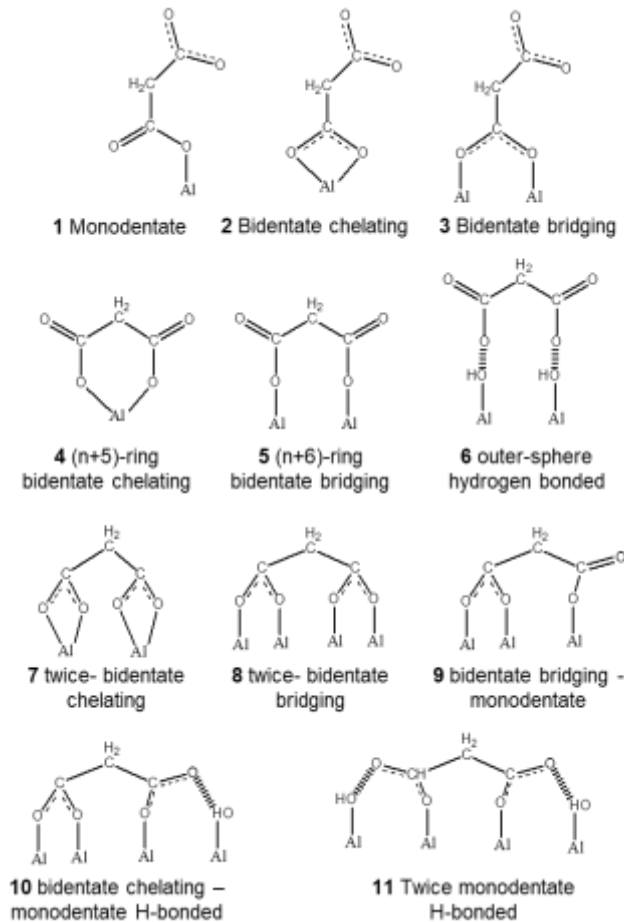
261

262

263 The *in situ* ATR-FT-IR characterization and adsorption isotherm give a first insight into the adsorption
 264 process of malonic acid at the solid/liquid interface. However, during a catalyst preparation using a pre-
 265 impregnation step a drying stage is often applied before the impregnation of active phase precursors.
 266 The adsorption mode of malonic acid could be impacted and needs to be determined after a drying
 267 stage and a subsequent creation of a solid/liquid interface during the impregnation.

268 **Adsorption mode of malonic acid**

269 Several adsorption modes of the protonated and deprotonated forms of malonic acid on mineral oxides
 270 surface are given in the literature⁴¹ (Figure 4). These modes differ by the number of carboxylate groups
 271 adsorbed at the metal oxide surface (one or two), the number of aluminum surface site involved, and
 272 the number of oxygen atoms per aluminum atom involved.



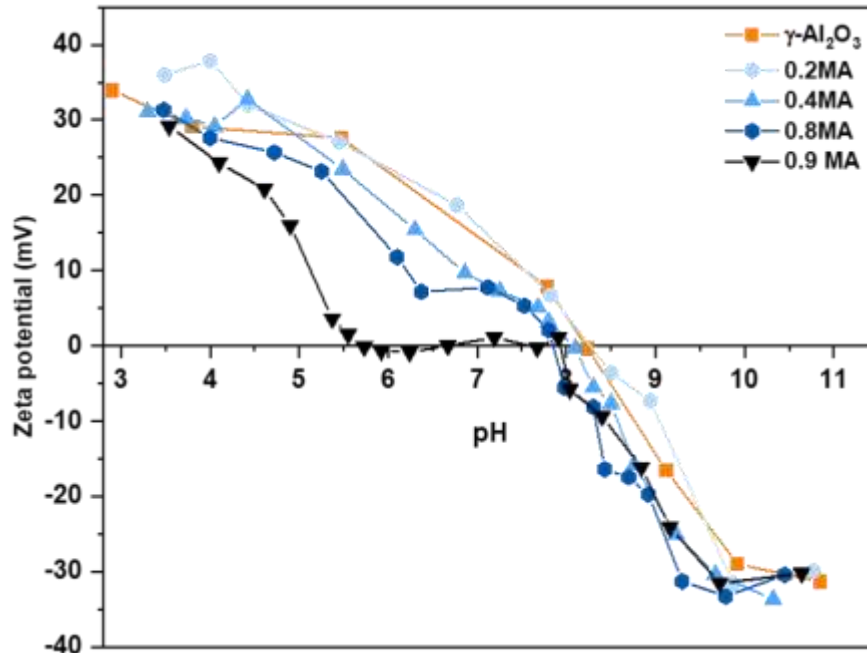
273

274 **Figure 4 : Potential adsorption modes for malonic acid adsorbed on alumina surface (modified scheme from Hug *et al.*⁴¹)**

275

276 Structures (1), (2) and (3) involve one carboxylate group, all the others involve two carboxylate groups
 277 (except for the outer-sphere hydrogen bonded complex (6)). Each carboxylate group can create one
 278 bond with one aluminum atom (monodentate), two bonds with the same aluminum atom (bidentate
 279 chelating) or each oxygen of the carboxylate group can create a bond with a different aluminum site
 280 (bidentate bridging).

281 As the impregnation isotherm indicates a specific adsorption, the surface sites density and charge
 282 should be impacted, and this modification can thus be monitored by zetametry. The Figure 5 presents
 283 the evolution of the zeta potential as a function of the pH and the malonic acid content.



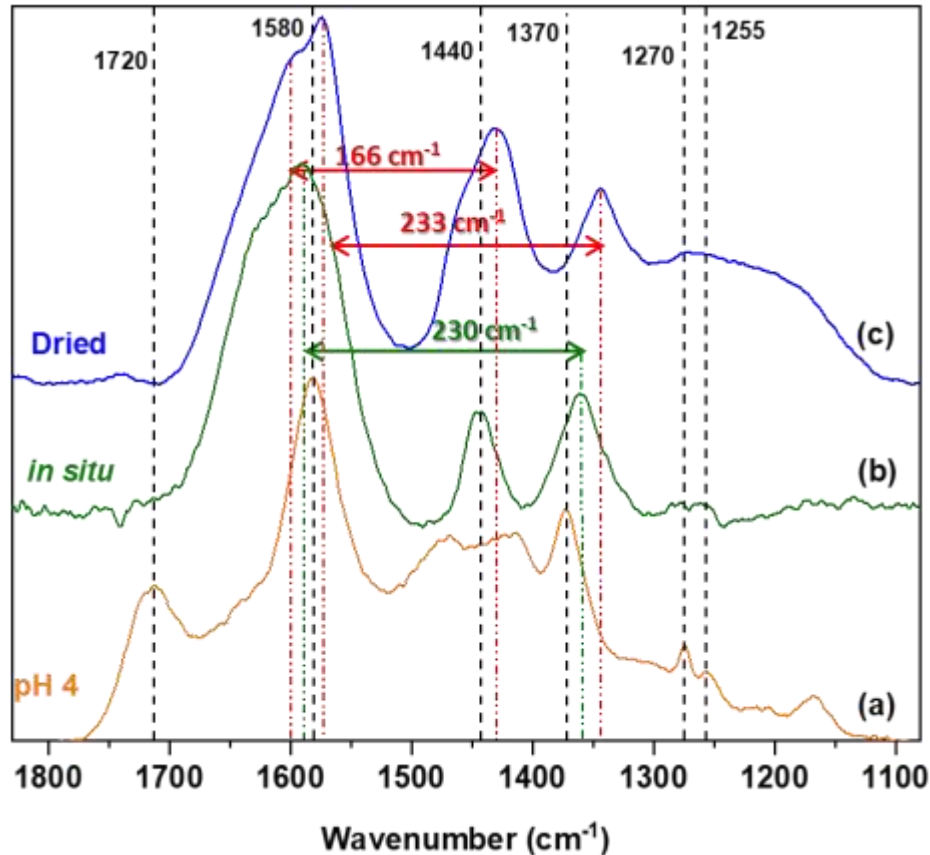
284

285 Figure 5 : Zeta potential as a function of pH for different surface coverages of malonic acid from 0 to 0.9 molecule/nm² (lines
286 are used as guidance for the reader)

287

288 The isoelectric point (IEP) of a solid (pH at $\zeta=0$ mV) is the result of the surface charge developed by the
289 surface sites and is characteristic of the oxide composition and structure. The change in the density of
290 surface hydroxyls by the specific adsorption of anionic species leads to a shift of the IEP towards lower
291 values^{42,43}. However, malonic acid has a peculiar impact on the zeta potential. Above 0.8
292 molecules/nm², a plateau in the zetametry curves starts to appear. At monolayer coverage, the plateau
293 has a zeta potential of zero and extends from pH 5.5 to 8. This observation indicates the presence of a
294 neutral surface complex with both carboxylate moieties bounded to the surface⁴⁴. Indeed, an ionisable
295 moiety would have led to the formation of a negative surface charge by deprotonation reaction (pK_{a2} is
296 equal to 5.3, see Figure 1) which is not compatible with a neutral zeta potential for a wide range of pH
297 values. Thus, the adsorption modes (1), (2) and (3) can be discarded among the different mechanisms
298 proposed in the literature (Figure 4). It should be noted that complete neutralization is only reached at
299 full monolayer coverage.

300 In an attempt to better understand the mechanisms, ATR-FT-IR spectra of the solution of malonic acid
301 at pH 4 (impregnation pH) have been compared to an *in situ* spectrum recorded at pH=4 (from Figure 2)
302 and to the one of the solid prepared by IWI and dried at 120°C (Figure 6). It should be noted that the
303 dried and *in situ* spectra correspond to different surface coverage, 0.9 and 0.2 malonic acid/nm²,
304 respectively. However, they could be compared as it could be considered that the surface speciation
305 does not evolve with the surface charge.



306

307 Figure 6 : ATR-FT-IR spectra of (a) malonic acid solution $C=0.1 \text{ mol L}^{-1}$ at $\text{pH}=4$ (b) malonic adsorbed on the alumina deposit
 308 (in situ experiment at $\text{pH}=4$) and (c) malonic acid adsorbed on $\gamma\text{-Al}_2\text{O}_3$ by IW1 ($\text{pH}=4$, $0.9 \text{ molecule/nm}^2$ and dried at 120°C for
 309 6 hours). All spectra are normalised to highest data point of each spectrum.

310


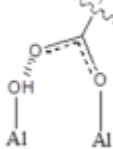
311 As already observed in the Figure 2, the malonic acid adsorption induces some spectral changes and the
 312 clear difference between the spectra of the solution and the complexes adsorbed on alumina (*in situ* or
 313 dried) supports a specific adsorption. First of all, the stretching mode of the HO-C=O (1720 cm^{-1}) is not
 314 present after adsorption indicating its participation to the adsorption process and thus its absence in
 315 the complex formed at the surface⁴¹. Then, adsorption modes schematized by structure (4), (5) and (9)
 316 in Figure 4 can be discarded. Secondly, the symmetric stretching mode of the COO group is shifted to
 317 lower value, from 1370 cm^{-1} to 1350 cm^{-1} which is in accordance with a specific interaction and
 318 confirmed that a formation of an outer-sphere hydrogen bonded complex is not the major adsorption
 319 mode, so the structure (6) can be discarded. Finally, the intensity of the CH_2 (1440 cm^{-1}) bending mode is
 320 enhanced after the adsorption. This latter modification is attributed in the literature^{13,45} to a
 321 geometrical constraint undergone by the CH_2 group that could be explained by the adsorption involving
 322 the two carboxylic groups. This hypothesis would also be consistent with the neutralization observed in
 323 the zetametry measurements. The Figure 6 (b) and (c) indicate that the drying slightly impacts the
 324 geometry of the complex formed at the surface. The main difference between the two spectra is the
 325 higher intensity of the CH_2 bending mode, which could be interpreted as a stronger geometric

326 constraint undergone by the CH₂ group and/or the presence of a symmetric COO stretching band under
 327 the latter.

328

329 The geometry of the complex can be refined using the difference between the asymmetric and
 330 symmetric stretching mode of COO as evocated by Dobson and McQuillan¹³. Indeed, this value is
 331 characteristic of the type of binding mode of the complex formed in solution or at the surface⁴⁰. Two
 332 adsorption modes of a carboxylic group can be distinguished, the bridging bidentate mode and the side
 333 on ester linkage with hydrogen bonding (Table 2), found in the adsorbed malonic complex 8-11 in Figure
 334 4.

335 **Table 2 : Adsorption mode of carboxylic acid group depending on the COO asymmetric and symmetric stretching mode**
 336 **difference**

Bridging Bidentate	Side on Ester linkage
$\Delta\nu(\text{COO})$ 150-180 cm ⁻¹ 	$\Delta\nu(\text{COO})$ > 208 cm ⁻¹ 

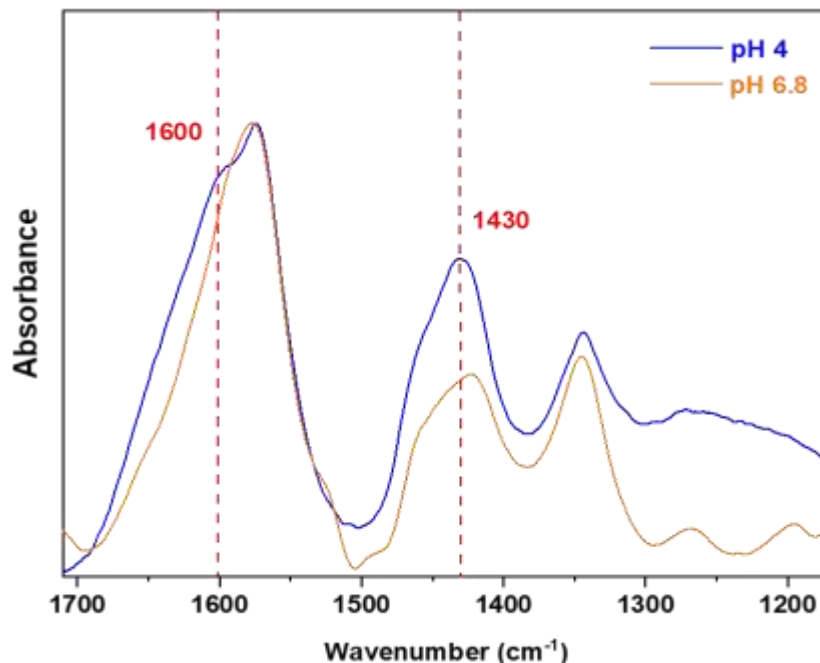
337

338

339 The wavenumber difference between the COO asymmetric and symmetric stretching modes $\Delta\nu(\text{COO})$
 340 varies from 150 to 180 cm⁻¹ for the bridging bidentate and is higher than 208 cm⁻¹ for the side on ester
 341 linkage (208 cm⁻¹ being the value in the dissolved dianion). By applying this rule to the *in situ* spectrum
 342 of adsorbed malonate (Figure 6 (b)), a difference of $\Delta\nu(\text{COO})=230$ cm⁻¹ is found in agreement with
 343 previous studies^{2,46}: both carboxylic moieties are mainly adsorbed through the same mode, the side on
 344 ester linkage (Figure 4 (11)). The carboxylic moiety adsorbs by sharing a hydrogen atom with an oxygen
 345 of the alumina surface, giving rise to a strong hydrogen bonding with similar features than
 346 carboxylate⁴⁷. This adsorption mode occurs directly at the wet interface and further drying stage
 347 removing water molecules can impact the geometry of the complex and bonding mode, contrary to the
 348 case of a bidentate bridging complex. Indeed, the spectra in Figure 6 (b) and (c) are slightly different.
 349 After the drying stage, a value for $\Delta\nu(\text{COO})$ of 166 cm⁻¹ could be measured, considering that the
 350 symmetric COO stretching is shifted towards higher wavenumbers at 1430 cm⁻¹. This indicates that the
 351 adsorption involved both a side-on ester linkage and a bidentate bridging mode after the drying of the
 352 solid in the same adsorption mode (Figure 4 (10)) or present in the several modes (Figure 4 (8) and
 353 (11)).

354 The adsorption mode has been determined during the equilibrium adsorption of the malonic acid as
 355 well as after a drying stage. Combining adsorption isotherm, zetametry measurements and ATR-FT-IR

356 characterizations, adsorption modes (1)-(7) and (9) have been discarded while three modes (8), (10) and
 357 (11) have been identified as possible structures of surface complex (Figure 4), with speciation being
 358 influenced by the drying stage. However, this drying influence seems absent when the impregnation is
 359 performed at a pH higher than pK_{a2} as illustrated on the Figure 7.



360

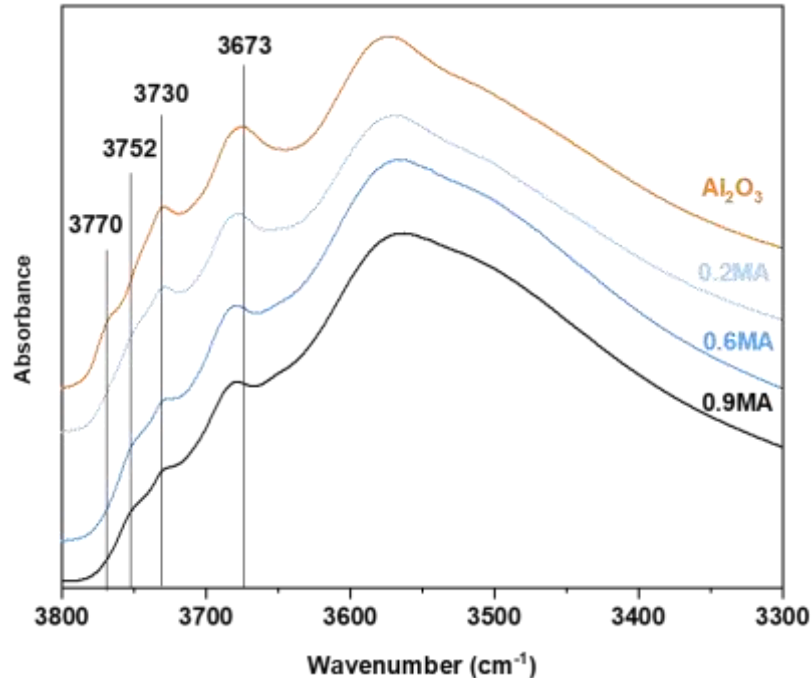
361 **Figure 7 : ATR-FT-IR spectra of dried support AcMalo/Al₂O₃ (0.9 molecule/nm²) prepared by IWI at different pH (4 and 6.8).**
 362 All spectra are normalized to highest data point of each spectrum.

363 Surprisingly, the pH seems to slightly impact the complex geometry after a drying stage which was not
 364 the case at the wet interface (Figure 2). It can be observed that a shoulder is developed at higher
 365 wavenumbers around 1600 cm⁻¹ for the asymmetric stretching mode of COO only at pH 4. This shoulder
 366 development is concomitant with the increasing intensity of the band situated at 1430 cm⁻¹ assigned to
 367 the CH₂ bending mode. This observation is a strong indication of the contribution of both the CH₂
 368 bending mode as well as the COO symmetric stretching mode to the 1430 cm⁻¹ band. The shoulder is
 369 absent for a pH above the second pKa ($pK_{a2}=5.7$) for supports impregnated by IWI and dried at 120°C
 370 for 6 hours. These observations can be linked to solution speciation. Indeed, at the impregnation
 371 conditions (2.9 mol L⁻¹ and pH 4), the monoacid form is the major species in solution, while the
 372 malonate (dianionic form) is the major one for a pH higher than pK_{a2} . During the impregnation, the
 373 buffer effect of the surface is expected to be strongly reduced by the high concentration of the malonic
 374 acid. The evolution of the pH has been simulated using PhreeqC, and the results have shown that it
 375 would evolve from 4 to 4.6 in presence of malonic acid, whereas it would reach 6.8 without it. The
 376 broadening of the band around 1600 cm⁻¹ could thus indicate an asymmetry of the two carboxylic
 377 groups present in the molecule at pH 4 leading to two different binding modes, the ester linkage mode
 378 with an hydrogen bond due to the carboxylate group and the bridging bidentate mode due to the
 379 carboxylic group. These adsorption modes can either be present in the same adsorption mode
 380 (structure (10), Figure 4) and/or in two different modes (structure (8) or (11), Figure 4).

381 As a result of the characterization techniques used, it has been seen that malonic acid adsorbs
382 specifically at the alumina surface through the formation of a neutral complex involving the two
383 carboxylic functions which leads to a geometric constraint on the CH₂ group by formation of both
384 bidentate bridging and ester linkage mode. Consequently, only 3 remaining adsorption modes can
385 correspond to these observations for impregnation at pH 4 (structures (8), (10) and (11), Figure 4). The
386 malonic acid reacts with one or different alumina surface hydroxyls to specifically adsorb at the surface.
387 Consequently, in order to fully describe the surface chemistry after modification, the determination of
388 the surface hydroxyls involved in the modification is necessary. To achieve this description, an
389 experimental technique (FT-IR) is merged with a surface complexation model at the alumina surface.

390 At an atomic scale, experimental works have shown the presence of various surface sites, especially by
391 the use of infrared spectroscopy. Morterra and Magnacca⁴⁸ showed the contribution of up to seven OH
392 groups. These surface hydroxyls are different by the charge developed which depends on the number of
393 bonds between the oxygen atom and aluminium atom(s) as well as on the aluminium coordination
394 (tetra-coordinated, penta-coordinated and hexa-coordinated). Research works from Digne *et al.*^{28,29}
395 allowed a construction of a description model of the γ -Al₂O₃ surface using DFT calculations which is
396 compared to an extensive list of published experimental data. The published model considers three
397 faces developed at the surface, (110), (100) and (111). The different types of hydroxyls can all be
398 considered as potential adsorption sites for malonic acid.

399 The spectra of dried samples have been recorded for malonic acid coverage from 0 up to 0.9 at/nm²
400 (Figure 8) after an activation at 120°C under vacuum (<10⁻⁵ mbar) in order to avoid the decomposition
401 of the organic at higher activation temperature. All spectra present large bands at 3770, 3752, 3730 and
402 3673 cm⁻¹ attributed Digne *et al.*^{28,29} respectively to the μ_1 -Al_V-OH (100), μ_3 -Al_V-OH (111), μ_1 -Al_V-OH
403 (110) and μ_2 -Al_V-OH (110).



404

405 **Figure 8 : Transmission FT-IR spectrum of γ - Al_2O_3 samples after malonic acid sorption and activation at 120 °C under vacuum**
 406 **(10^{-5} mbar), OH stretch region**

407

408 The decrease of the intensity of all bands observed on the Figure 8 seems to indicate that all surface
 409 hydroxyls corresponding to bands between 3650 and 3800 cm^{-1} are involved in the adsorption of
 410 malonic acid (see also the difference spectra in the supporting information, Figure S1). Only one band,
 411 at 3752 cm^{-1} seems to grow a little but it could be explained by the decrease of the overlapping
 412 neighbouring bands. However, at the monolayer coverage, infrared bands are still present, i.e. they are
 413 not fully consumed confirming that the maximum coverage of the adsorbate is smaller than the surface
 414 hydroxyl density⁴⁹. Due to the presence of residual water molecules at the surface, the resolution of the
 415 bands is not very high and a detailed interpretation of the spectra is delicate. The crucial information
 416 obtained from these spectra is the consumption of several surface hydroxyls present on two main
 417 facets of alumina, (110) and (100). However, the description of the surface sites involved in the
 418 adsorption of malonic acid cannot be directly derived from the FT-IR spectra alone, as the hydroxyl
 419 sites' density and reactivity are very sensitive to the hydration state of the surface. The hydration state
 420 corresponding to FT-IR conditions is different from the one encountered during the wet impregnation
 421 process, hence the nature of the surface OH groups is not the same and the coordination sphere of the
 422 surface Al atoms changes. When it comes to rationalize surface complexation phenomena according to
 423 the so-called MUSIC complexation model^{37,50}, the protonation constants of surface hydroxo groups
 424 depend on the local charge thus, on the coordination number of the host surface cations holding these
 425 reactive groups. Consequently, the use of a surface complexation model involving a hydrated alumina
 426 surface is necessary to identify the hydroxyls responsible for the adsorption at the solid/liquid interface.

427 The model of γ -alumina hydrated surface used in this surface complexation model is the one developed
428 by some of us in reference ³² from the simulation of the acid-base titration curve of the surface. This
429 model is based on DFT information^{28,29} (density and charge of each site) and the MUSIC model^{51,52} to
430 determine the pKa of each hydroxyl site (Table S1 and S2 in the supporting information). The model
431 includes the two most developed facets on the alumina surfaces, the (100) and (110) orientations, in
432 their respective proportion^{28,53} (20 and 80% respectively) and with their hydroxyl content and structure
433 at the solid/liquid interface. The main differences, between the model that is relevant at FT-IR
434 conditions and the one used here for the interpretation of zetametry experiments, are a higher OH
435 content and the full saturation of the coordination spheres of surface Al sites in the latter model, which
436 influences the surface protonation constants. Moreover, to describe the complete solid/solution
437 surface charge as a function pH, all this information has been implemented into surface speciation
438 calculations made by means of the PHREEQC2 software⁵⁴ and applying a basic Stern double layer model.

439 Our model considers several hypotheses based on the literature and on our results obtained by surface
440 characterization experiments. Firstly, no protonation/deprotonation constant has been implemented
441 on the adsorbed surface complex due to the neutrality plateau observed by zetametry experiments in
442 the pH range between 5.5 and 8.0 (Figure 5) and the participation of the two carboxylic groups
443 according to ATR-FT-IR (Figure 6 and Table 2). Secondly, malonic acid adsorption is considered as
444 irreversible due to its specific adsorption, since only a small quantity of malonate adsorbed is released
445 after an application of a drying stage and a washing stage regardless of the pH of the washing solution
446 (Figure S3).

447 The use of this model does not imply any fitting procedure as the main objective is to reproduce the
448 evolution of the zetametry curve with increasing malonate content. Thus, by comparing our data with
449 scenarios implying a specific and successive consumption of surface sites, we firstly aim to simulate the
450 neutralization plateau observed in zetametry and secondly model the curve progression of the
451 experimental zetametry measurements observed in Figure 5.

452 Several scenarios have been tested to retrieve the characteristic neutralization plateau observed at the
453 monolayer coverage during the zetametry measurements (Figure S2). The curve in Figure 9 represents
454 the closest simulation to the experiment. Some differences exist between simulated and measured zeta
455 potential curves which mostly consists in a shift of surface charge at pH above 8, i.e. in the domain
456 where the malonate adsorption becomes negligible. This difference already existed in the original
457 model (where only the (de)protonation of the hydroxyl groups was simulated) and has no impact for
458 the determination of the geometry of the malonate surface complex.

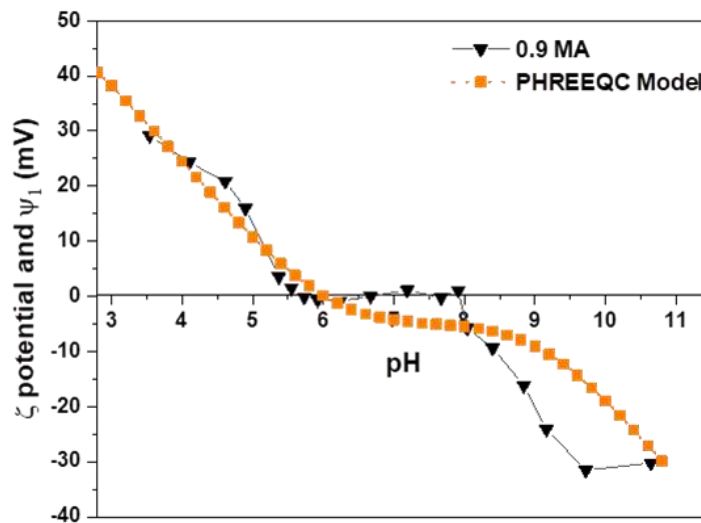
459 To obtain the plateau (Figure 9), we had to distinguish between the reactivity of the two facets of γ -
460 Al_2O_3 particles. Thus, all the hydroxyl sites on the (100) facet need to be involved whereas only the μ_1 -
461 Al-OH (IV and VI) of the (110) facet are consumed by the adsorption (Table 3). The involvement of these
462 two latter sites is not surprising as they are one the most basic (reactive) surface hydroxyls. The total
463 density of surface sites involved is 3.2 OH/nm² corresponding to 3.5 OH/molecule adsorbed (with 0.9
464 molecule/nm² as monolayer coverage content) which is coherent with the structure mode ((8) and (10),

465 Figure 4) since the surface complexes formed consume between 3 (structure 10)) and 4 (structure (8))
 466 surface hydroxyls.

467 **Table 3 : Characteristics of γ -Al₂O₃ surface -OH groups at different malonic acid coverage (from 0 to 100%) for the (100) and**
 468 **(110) orientations taking into account the facets proportion.**

Surface Coverage	Surface sites density (at/nm ²)							
	(100)			(110)				
	μ_1 -Al _{VI}	μ_2 -Al _{VI} - Al _{IV}	μ_3 -Al _{VI}	μ_1 -Al _{IV}	μ_1 -Al _{VI}	μ_2 -Al _{VI} - Al _{IV}	μ_2 -Al _{VI} - Al _{VI}	μ_3 -Al _{VI}
0%	0.43	0.22	0.22	1.19	1.19	2.38	1.19	1.19
20%	0.35	0.17	0.17	0.95	0.95	2.38	1.19	1.19
40%	0.26	0.13	0.13	0.71	0.71	2.38	1.19	1.19
60%	0.17	0.09	0.09	0.48	0.48	2.38	1.19	1.19
80%	0.09	0.04	0.04	0.24	0.24	2.38	1.19	1.19
100%	0.00	0.00	0.00	0.00	0.00	2.38	1.19	1.19

469



470

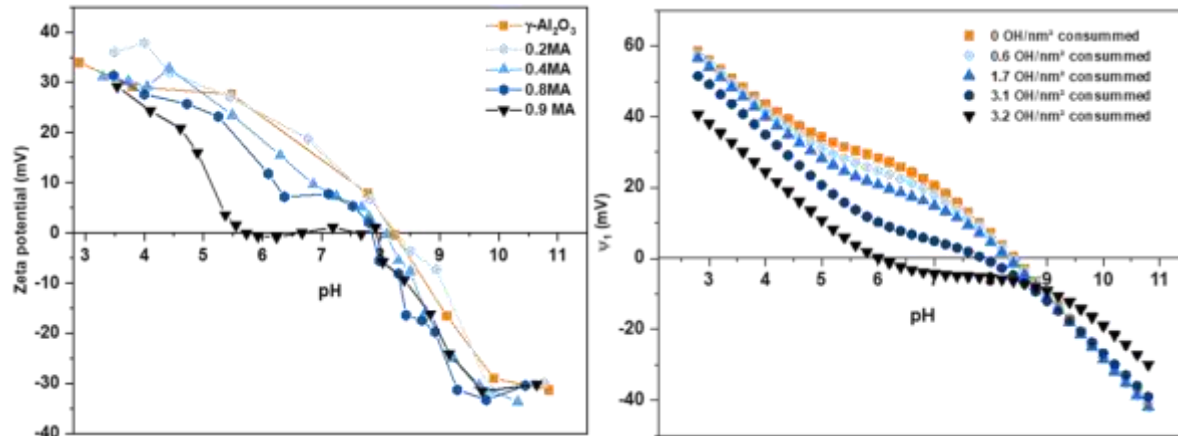
471 **Figure 9 : Evolution of the ζ potential as a function of pH for alumina modified by malonic acid compared to experimental**
 472 **data**

473

474 The second information that the model can illustrate here is the reactivity of the sites involved in the
 475 monolayer coverage formation. Indeed, it has been highlighted that only the consumption of specific
 476 surface sites allows retrieving the evolution of the zetametry curves as a function of increasing surface
 477 coverage observed experimentally (Figure 10). Concerning the adsorption sites needed to model the
 478 plateau, the results indicate that none of these adsorption sites are more reactive than the others (the
 479 average site consumption as a malonic acid coverage increases is the same for all sites), as only a
 480 continuous decrease of all sites involved makes it possible to retrieve the curves' evolution. This result is
 481 consistent with FT-IR data where the evolution of the different bands as function of malonate content
 482 shows a continuous decrease. Thus, according to these results, the involved sites present similar
 483 reactivity. However, the consequences of malonic acid adsorption, and the resulting surface properties

484 after the adsorption process, are expected to be different for the two facets: in the (100) orientation all
 485 OH groups are consumed whereas in the (110) facet only two μ_1 sites are involved and the remaining
 486 μ_2 and μ_3 remain unconsumed.

487



488

489 **Figure 10 :** (A) Zeta potential as a function of pH for different contents of malonic acid from 0 to 0.9 molecule/nm² (lines are
 490 used as guidance for the reader) (B) Calculated ψ_1 as a function of pH for different content of surface hydroxyls consumed
 491 (from 0 to 3.2 OH/nm²)

492

493 Consequently, the model presented here supports the determination of the complex adsorption modes
 494 obtained by experimental characterization but also helps to get more specific information on the
 495 adsorption process by identifying the surface hydroxyls involved in the adsorption and their reactivity.
 496 To the best of our knowledge, this is the first time the adsorption of malonic acid (carboxylic acid) is so
 497 deeply characterized by both its surface complex geometry and the sites responsible for its adsorption.

498

499 Conclusion

500 The complementarity between the use of multi-technique characterization and modelling has been
 501 demonstrated here by the description at the molecular level of a modified γ -Al₂O₃ surface with malonic
 502 acid. The surface complex geometry was determined via the coupling of adsorption isotherm, zetametry
 503 measurements and ATR-FT-IR characterization. The complex involves two types of carboxylate bonding,
 504 bridging bidentate and side-on ester linkage leading to a neutral complex at the surface. The infrared
 505 characterization even underlined a slight drying effect on the geometry of the adsorbed complex
 506 probably due the removal of water molecule. The results presented here show that the progressive
 507 coverage of the surface by malonic acid ψ complex neutralized the surface once the monolayer coverage
 508 content of 0.9 molecule/nm² is achieved by the consumption of specific surface sites. The whole (100)
 509 facet is reactive towards the adsorption while only μ_1 -Al_{IV}-OH and μ_1 -Al_{IV}-OH are involved on the (110)
 510 facet. It also helps to support the complex geometry defined via experimental infrared data, i.e. a

511 consumption of 3.5 OH/molecule, in coherence with the two proposed structures for the adsorption
512 mode.

513 This work helps to obtain a high level of detail on the adsorption of a dicarboxylic acid on an oxide
514 surface by including the monolayer coverage content, the surface sites and facets involved in the
515 adsorption and the surface complex geometry. The molecular description of the modified alumina
516 surface will allow the preparation of catalyst with defined surface chemistry, a useful strategy to
517 understand the impact of the latter during the different preparation steps and on the catalytic
518 performance.

519

520

521

522 Bibliography

- 523 (1) Gadd, G. M. Biosorption : Critical Review of Scientific Rationale, Environmental Importance and
524 Significance for Pollution Treatment. *J. Chem. Technol. Biotechnol.* **2009**, No. 84, 13–28.
- 525 (2) Patel, M. A.; Kar, A. S.; Raut, V. V; Tomar, B. S. Probing and Understanding Interaction of Eu (III)
526 with γ -Alumina in Presence of Malonic Acid. *J. Environ. Sci.* **2021**, *100*, 181–192.
- 527 (3) Mazoyer, P.; Geantet, C.; Diehl, F.; Loridant, S.; Lacroix, M. Role of Chelating Agent on the Oxidic
528 State of Hydrotreating Catalysts. *Catal. Today* **2008**, *130* (1), 75–79.
- 529 (4) Chen, J.; Mi, J.; Li, K.; Wang, X.; Dominguez Garcia, E.; Cao, Y.; Jiang, L.; Oliviero, L.; Maugé, F.
530 Role of Citric Acid in Preparing Highly Active CoMo/Al₂O₃ Catalyst: From Aqueous Impregnation
531 Solution to Active Site Formation. *Ind. Eng. Chem. Res.* **2017**, *56* (48), 14172–14181.
- 532 (5) Lambert, J.; Che, M. The Molecular Approach to Supported Catalysts Synthesis : State of the Art
533 and Future Challenges. *J. Mol. Catal. A Chem.* **2000**, No. 162, 5–18.
- 534 (6) Sun, M.; Nicosia, D.; Prins, R. The Effects of Fluorine, Phosphate and Chelating Agents on
535 Hydrotreating Catalysts and Catalysis. *Catal. Today* **2003**, *86* (1–4), 173–189.
- 536 (7) Caloch, B.; Rana, M. S.; Ancheyta, J. Improved Hydrogenolysis (C-S, C-M) Function with Basic
537 Supported Hydrodesulfurization Catalysts. *Catal. Today* **2004**, *98* (1-2 SPEC. ISS.), 91–98.
- 538 (8) Rana, M. S.; Ramírez, J.; Gutiérrez-Alejandre, A.; Ancheyta, J.; Cedeño, L.; Maity, S. K. Support
539 Effects in CoMo Hydrodesulfurization Catalysts Prepared with EDTA as a Chelating Agent. *J.*
540 *Catal.* **2007**, *246* (1), 100–108.
- 541 (9) Koizumi, N.; Mochizuki, T.; Yamada, M. Preparation of Highly Active Catalysts for Ultra-Clean
542 Fuels. *Catal. Today* **2009**, *141* (1–2), 34–42.
- 543 (10) Munnik, P.; De Jongh, P. E.; De Jong, K. P. Recent Developments in the Synthesis of Supported
544 Catalysts. *Chem. Rev.* **2015**, *115* (14), 6687–6718.

- 545 (11) Hou, Z.; McConnachie, J. M.; Mizan, T.; Borghard, W. G.; Lewis, W. E.; Ismail, N. S.; Dandekar, A.
546 B. Hydroprocessing Methods for Bulk Group VIII/VIB Metal Catalysts. WO Patent 2008/045550,
547 2009.
- 548 (12) Klimov, O. V.; Pashigreva, A. V.; Fedotov, M. A.; Kochubey, D. I.; Chesalov, Y. A.; Bukhtiyarova, G.
549 A.; Noskov, A. S. Co-Mo Catalysts for Ultra-Deep HDS of Diesel Fuels Prepared via Synthesis of
550 Bimetallic Surface Compounds. *J. Mol. Catal. A Chem.* **2010**, 322 (1–2), 80–89.
- 551 (13) Dobson, K. D.; McQuillan, A. J. In Situ Infrared Spectroscopic Analysis of the Adsorption of
552 Aromatic Carboxylic Acids to TiO₂, ZrO₂, Al₂O₃, and Ta₂O₅ from Aqueous Solutions. *Spectrochim.*
553 *Acta - Part A Mol. Biomol. Spectrosc.* **2000**, 56 (3), 557–565.
- 554 (14) Anaya, S.; Serrano, B.; Herrero, B.; Cervera, A.; Baselga, J. γ -Alumina Modification With Long
555 Chain Carboxylic Acid Surface Nanocrystals for Biocompatible Polysulfone Nanocomposites. *ACS*
556 *Appl. Mater. Interfaces* **2014**, 6 (16), 14460–14468.
- 557 (15) Davantès, A.; Schlaup, C.; Carrier, X.; Rivallan, M.; Lefèvre, G. In Situ Cobalt Speciation on γ -Al₂O₃
558 in the Presence of Carboxylate Ligands in Supported Catalyst Preparation. *J. Phys. Chem. C* **2017**,
559 121 (39), 21461–21471.
- 560 (16) Klimov, O. V.; Vatutina, Y. V.; Nadeina, K. A.; Kazakov, M. O.; Gerasimov, E. Y.; Prosvirin, I. P.;
561 Larina, T. V.; Noskov, A. S. CoMoB/Al₂O₃ Catalysts for Hydrotreating of Diesel Fuel. The Effect of
562 the Way of the Boron Addition to a Support or an Impregnating Solution. *Catal. Today* **2018**, 305,
563 192–202.
- 564 (17) Rinaldi, N. Preparation of Highly Active CoMo/Al₂O₃ HDS Catalysts with Citric Acid Addition by
565 the Post-Treatment Method. *Indones. J. Chem.* **2010**, 10 (3), 341–347.
- 566 (18) Suárez-Toriello, V. A.; Santolalla-Vargas, C. E.; De Los Reyes, J. A.; Vázquez-Zavala, A.; Vrinat, M.;
567 Geantet, C. Influence of the Solution PH in Impregnation with Citric Acid and Activity of
568 Ni/W/Al₂O₃ Catalysts. *J. Mol. Catal. A Chem.* **2015**, 404–405, 36–46.
- 569 (19) Escobar, J.; Barrera, M. C.; Gutiérrez, A. W.; Terrazas, J. E. Benzothiophene Hydrodesulfurization
570 over NiMo/Alumina Catalysts Modified by Citric Acid. Effect of Addition Stage of Organic
571 Modifier. *Fuel Process. Technol.* **2017**, 156, 33–42.
- 572 (20) Lan, Y.; Li, C.; Mao, J.; Sun, J. Influence of Clay Minerals on the Reduction of Cr⁶⁺ by Citric Acid.
573 *Chemosphere* **2008**, 71 (4), 781–787.
- 574 (21) Hug, S. J.; Laubscher, H. U.; James, B. R. Iron(III) Catalyzed Photochemical Reduction of
575 Chromium(VI) by Oxalate and Citrate in Aqueous Solutions. *Environ. Sci. Technol.* **1997**, 31 (1),
576 160–170.
- 577 (22) Abrahamson, H. B.; Rezvani, A. B.; Brushmiller, J. G. Photochemical and Spectroscopic Studies of
578 Complexes, of Iron(III) with Citric Acid and Other Carboxylic Acids. *Inorganica Chim. Acta* **1994**,
579 226 (1–2), 117–127.
- 580 (23) Jansen, M. A.; van Houtert, F. W.; Ado, T.; Kamo, T.; Nishimoto, N. Process for Activating a
581 Hydrotreating Catalyst. U.S. Patent 7,956,000 B2, 2007.

- 582 (24) Eijsbouts, S.; Wilhelmus Houtert, F.; Jansen, M.; Kamo, T.; Plantenga, F. Process for Regenerating
583 Additive-Based Catalysts. U.S. Patent 6,635,596, 2003.
- 584 (25) Marafi, M. A.; Stanislaus, A.; Mumford, C. J.; Fahim, M. Rejuvenation of Spent Residue
585 Hydroprocessing Catalyst by Leaching of Foulant Metals. *Stud. Surf. Sci. Catal.* **1989**, *53* (C), 213–
586 223.
- 587 (26) McCarthy, S. J.; Bai, C.; BORGHARD, W. G.; Lewis, W. E. Regeneration and Rejuvenation of
588 Supported Hydroprocessing Catalysts. WO Patent 2009/126278 A3, 2009.
- 589 (27) Kummert, R.; Stumm, W. The Surface Complexation of Organic Acids on Hydrous γ -Al₂O₃. *J.*
590 *Colloid Interface Sci.* **1980**, *75* (2), 373–385.
- 591 (28) Digne, M.; Sautet, P.; Raybaud, P.; Euzen, P.; Toulhoat, H. Hydroxyl Groups on γ -Alumina
592 Surfaces : A DFT Study. *J. Catal.* **2002**, *211*, 1–5.
- 593 (29) Digne, M.; Sautet, P.; Raybaud, P.; Euzen, P.; Toulhoat, H. Use of DFT to Achieve a Rational
594 Understanding of Acid-Basic Properties of γ -Alumina Surfaces. *J. Catal.* **2004**, *226*, 54–68.
- 595 (30) Réocreux, R.; Jiang, T.; Iannuzzi, M.; Michel, C.; Sautet, P. Structuration and Dynamics of
596 Interfacial Liquid Water at Hydrated γ -Alumina Determined by Ab Initio Molecular Simulations:
597 Implications for Nanoparticle Stability. *ACS Appl. Nano Mater.* **2018**, *1* (1), 191–199.
- 598 (31) Nguouana-Wakou, B. F.; Cornette, P.; Corral Valero, M.; Costa, D.; Raybaud, P. An Atomistic
599 Description of the γ -Alumina/Water Interface Revealed by Ab Initio Molecular Dynamics. *J. Phys.*
600 *Chem. C* **2017**, *121* (19), 10351–10363.
- 601 (32) Corral Valero, M.; Prelot, B.; Lefèvre, G. MUSIC Speciation of γ -Al₂O₃ at the Solid Liquid Interface:
602 How DFT Calculations Can Help with Amorphous and Poorly Crystalline Materials. *Langmuir*
603 **2019**, *35* (40), 12986–12992.
- 604 (33) Karaman, M. E.; Antelmi, D. A.; Pashley, R. M. The Production of Stable Hydrophobic Surfaces by
605 the Adsorption of Hydrocarbon and Fluorocarbon Carboxylic Acids onto Alumina Substrates.
606 *Colloids Surfaces A Physicochem. Eng. Asp.* **2001**, *182*, 285–298.
- 607 (34) Park, J.; Regalbuto, J. R. A Simple, Accurate Determination of Oxide PZC and the Strong Buffering
608 Effect of Oxide Surfaces at Incipient Wetness. *J. Colloid Interface Sci.* **1995**, *175*, 239–252.
- 609 (35) Roy, T.; Wisser, D.; Rivallan, M.; Valero, M. C.; Corre, T.; Delpoux, O.; Pirngruber, G. D.; Lefèvre,
610 G. Phosphate Adsorption on γ - Alumina: A Surface Complex Model Based on Surface
611 Characterization and Zeta Potential Measurements. *J. Phys. Chem. C.* **2021**.
- 612 (36) Mayordomo, N.; Foerstendorf, H.; Lützenkirchen, J.; Heim, K.; Weiss, S.; Alonso, U.; Missana, T.;
613 Schmeide, K.; Jordan, N. Selenium(IV) Sorption Onto γ -Al₂O₃: A Consistent Description of the
614 Surface Speciation by Spectroscopy and Thermodynamic Modeling. *Environ. Sci. Technol.* **2018**,
615 *52* (2), 581–588.
- 616 (37) Hiemstra, T.; Yong, H.; Riemsdijk, W. H. Van. Interfacial Charging Phenomena of Aluminum
617 (Hydr) Oxides. *Langmuir* **1999**, *15*, 5942–5955.
- 618 (38) Kettler, R. M.; Wesolowski, D. J.; Palmer, D. A. Dissociation Quotients of Malonic Acid in Aqueous

- 619 Sodium Chloride Media to 100°C. *J. Solution Chem.* **1992**, 21 (8), 883–900.
- 620 (39) Persson, P.; Axe, K. Adsorption of Oxalate and Malonate at the Water-Goethite Interface :
621 Molecular Surface Speciation from IR Spectroscopy. *Geochim. Cosmochim. Acta* **2005**, 69 (3),
622 541–552.
- 623 (40) Lefèvre, G.; Preočanin, T.; Lützenkirchen, J. Attenuated Total Reflection - Infrared Spectroscopy
624 Applied to the Study of Mineral - Aqueous Electrolyte Solution Interfaces: A General Overview
625 and a Case Study. In *Infrared Spectroscopy - Materials Science, Engineering and Technology*;
626 Theophanides, T., Ed.; Infrared Spectroscopy, Intech, 2012; Vol. 1, pp 97–122.
- 627 (41) Hug, S. J.; Bahnemann, D. Infrared Spectra of Oxalate , Malonate and Succinate Adsorbed on the
628 Aqueous Surface of Rutile , Anatase and Lepidocrocite Measured with in Situ ATR-FTIR. **2006**,
629 *150*, 208–219.
- 630 (42) Cordero, R. L.; Gil Llambías, F. J.; Palacios, J. M.; Fierro, J. L. G.; Agudo, A. L. Surface Changes of
631 Alumina Induced by Phosphoric Acid Impregnation. *Appl. Catal.* **1989**, 56 (1), 197–206.
- 632 (43) Spanos, N.; Slavov, S.; Kordulis, C.; Lycourghiotis, A. Mechanism of Deposition of the CrO_4^{2-} ,
633 HCrO_4^- , and $\text{Cr}_2\text{O}_7^{2-}$ Ions on the γ -Alumina Surface. *Langmuir* **1994**, 10 (9), 3134–3147.
- 634 (44) Mansour, C.; Lefèvre, G.; Pavageau, E. M.; Catalette, H.; Fédoroff, M.; Zanna, S. Journal of Colloid
635 and Interface Science Sorption of Sulfate Ions onto Magnetite. *J. Colloid Interface Sci.* **2009**, 331
636 (1), 77–82.
- 637 (45) Lenhart, J. J.; Bargar, R. J.; Davis, A. J. Spectroscopic Evidence for Ternary Surface Complexes in
638 the Lead (II)-Malonic Acid-Hematite System. *J. Colloid Interface Sci.* **2001**, 234 (2), 448–452.
- 639 (46) Duckworth, O. W.; Martin, S. T. Surface Complexation and Dissolution of Hematite by C1-C6
640 Dicarboxylic Acids at pH5.0 . *Geochim. Cosmochim. Acta* **2001**, 65 (23), 4289–4301.
- 641 (47) Mao, Y.; Fung, B. M. A Study of the Adsorption of Acrylic Acid and Maleic Acid from Aqueous
642 Solutions onto Alumina. *J. Colloid Interface Sci.* **1997**, 221 (191), 216–221.
- 643 (48) Morterra, C.; Magnacca, G. A Case Study : Surface Chemistry and Surface Structure of Catalytic
644 Aluminas , as Studied by Vibrational Spectroscopy of Adsorbed Species. *Catal. Today* **1996**, 27,
645 497–532.
- 646 (49) Lützenkirchen, J.; Boily, J. F.; Lövgren, L.; Sjöberg, S. Limitations of the Potentiometric Titration
647 Technique in Determining the Proton Active Site Density of Goethite Surfaces. *Geochim.*
648 *Cosmochim. Acta* **2002**, 66 (19), 3389–3396.
- 649 (50) Hiemstra, T.; de Wit, J. C. M.; van Riemsdijk, W. H. Multisite Proton Adsorption Modeling at the
650 Solid/Solution Interface of (Hydr)Oxides: A New Approach II. Application to Various Important
651 (Hydr)Oxides. *J. Colloid Interface Sci.* **1989**, 133 (1), 105–117.
- 652 (51) Hiemstra, T.; Venema, P.; Van Riemsdijk, W. H. Intrinsic Proton Affinity of Reactive Surface
653 Groups of Metal (Hydr)Oxides: The Bond Valence Principle. *J. Colloid Interface Sci.* **1996**, 184,
654 680–692.

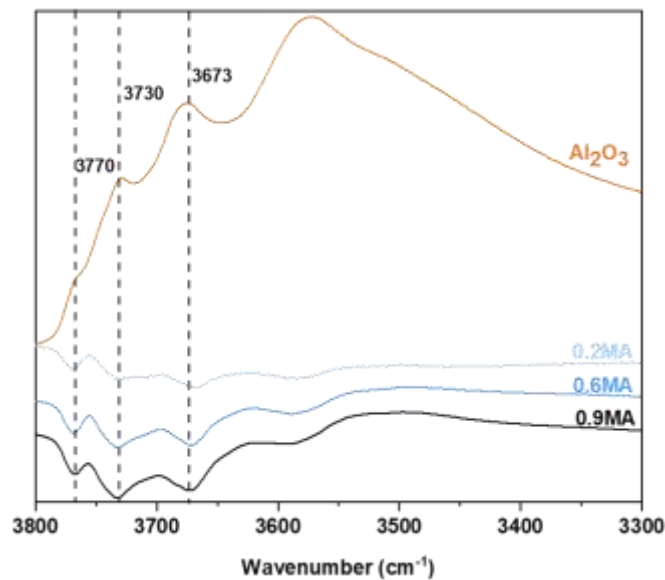
- 655 (52) Hiemstra, T.; Wolthers, M. A Surface Structural Approach to Ion Adsorption: The Charge
656 Distribution (CD) Model. *J. Colloid Interface Sci.* **1996**, *179* (179), 488–508.
- 657 (53) Beaufils, J.; Barbaux, Y. Détermination, Par Diffraction Differentielle de Neutrons, Des Faces
658 Cristallines Exposées Par Des Supports de Catalyseurs En Poudre. *J. Chim. Phys.* **1981**, *78* (4),
659 347–352.
- 660 (54) Parkhurst, D. L.; Appelo, C. A. J. User's Guide to PHREEQC (Version 2) - A Computer Program for
661 Speciation, Batch Reaction, One-Dimensional Transport, and Inverse Geochemical Calculations.
662 *Water Resour. Investig.* **1999**, No. USGS.
- 663
- 664

665 **Malonate speciation at γ -alumina surface using surface complex**
 666 **modelling based on a multi-technique characterization approach**
 667 Teddy Roy, Manuel Corral Valero, Thibaut Corre, Olivier Delpoux, Gerhard Pirngruber, Grégory Lefèvre

668 **SUPPORTING INFORMATION**

669

670



671

672 **Figure S1 : Transmission FT-IR difference spectra between γ - Al_2O_3 and alumina impregnated with malonic acid at different**
 673 **content (from 0.2 to 0.9 at/nm²) after activation at 120°C under vacuum (10⁻⁵ mbar), OH stretching region.**

674

675

676

677 **Table S1: Characteristics of γ - Al_2O_3 Surface -OH groups at water coverage of 0.17 and 0.18 OH/nm² for the (100) and (110)**
 678 **orientations¹**

OH site	Al involved	Surface density (nm ⁻²)	
		(100)	(110)
H ₂ O	Al _{VI}	2.17	4.48
μ_1	Al _{VI}	2.17	1.49
μ_1	Al _{IV}	0	1.49
μ_2	Al _{VI} and Al _{IV}	1.09	2.98
μ_2	Only Al _{VI}	0	1.49
μ_3	Only Al _{VI}	1.09	1.49

679

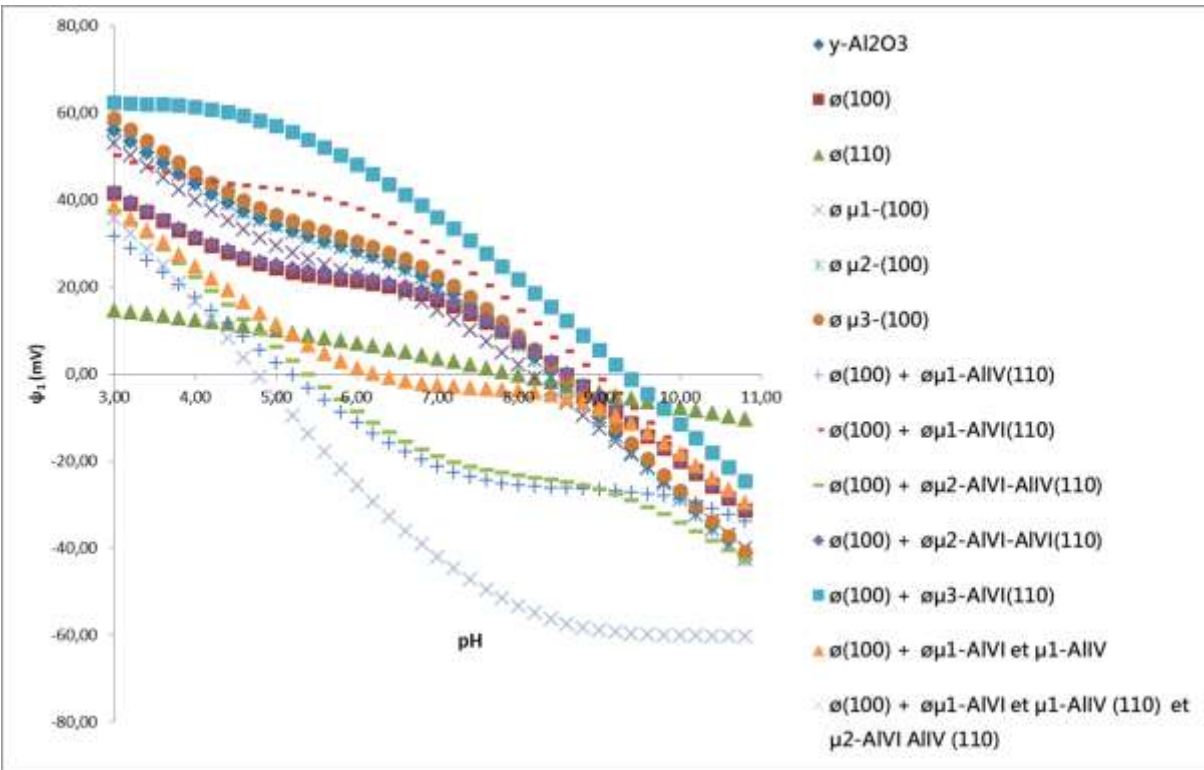
680

681

682 **Table S2: Calculation of Protonation Constants Using AIMD Simulations To Determine the Number of H Bonds around**
 683 **Oxygen Atoms in Hydroxyl Groups (a + d) and the number of H bonds around their respective protons (p)¹**

OH site	Al involved	Protonation reaction	Log K	Nb of H bonds with the proton
Surface (100)				
μ_1	Al _{VI}	$\mu_1\text{OH}^{-0.5} + \text{H}^+ \rightleftharpoons \mu_1\text{OH}_2^{+0.5}$	8.16	0.86
μ_2	Al _{VI} - Al _{IV}	$\mu_2\text{O}^{-0.75} + \text{H}^+ \rightleftharpoons \mu_2\text{OH}^{+0.25}$	10.32	n.a.
μ_3	Al _{VI}	$\mu_3\text{O}^{-0.5} + \text{H}^+ \rightleftharpoons \mu_3\text{OH}^{+0.5}$	5.94	n.a.
Surface (110)				
μ_1	Al _{IV}	$\mu_1\text{OH}^{-0.25} + \text{H}^+ \rightleftharpoons \mu_1\text{OH}_2^{+0.75}$	0.12	0.75
μ_1	Al _{IV}	$\mu_1\text{O}^{-1.25} + \text{H}^+ \rightleftharpoons \mu_1\text{OH}^{-0.25}$	12.97	n.a.
μ_1	Al _{VI}	$\mu_1\text{OH}^{-0.5} + \text{H}^+ \rightleftharpoons \mu_1\text{OH}_2^{+0.5}$	9.16	0.95
μ_2	Al _{VI} - Al _{IV}	$\mu_2\text{O}^{-0.75} + \text{H}^+ \rightleftharpoons \mu_2\text{OH}^{+0.25}$	10.45	n.a.
μ_2	Al _{VI} - Al _{VI}	$\mu_2\text{OH}^0 + \text{H}^+ \rightleftharpoons \mu_2\text{OH}_2^{+1}$	0.29	0.57
μ_2	Al _{VI} - Al _{VI}	$\mu_2\text{O}^{-1} + \text{H}^+ \rightleftharpoons \mu_2\text{OH}^0$	13.86	n.a.
μ_3	Al _{VI}	$\mu_3\text{O}^{-0.5} + \text{H}^+ \rightleftharpoons \mu_3\text{OH}^{+0.5}$	4.75	n.a.

684



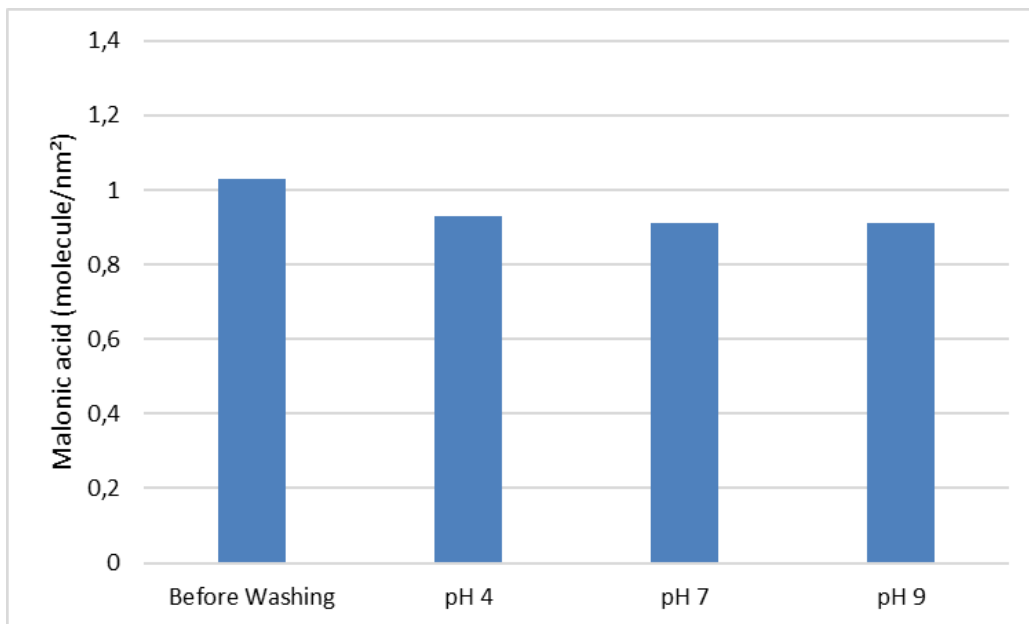
685

686

687

Figure S2: PHREEQC simulations of the ψ_1 evolution as a function of pH for different scenarios after surface sites removal of the $\gamma\text{-Al}_2\text{O}_3$ model (\emptyset = removal of sites of this face)

688



689

690

Figure S311 : Malonic acid content (molecule/nm²) obtained after a washing stage at different pH

691

692 PHREEQC Script

```

693
694 TITLE CD-MUSIC alumina_Malonic_acid
695
696 PHASES
697 Fix_H+
698     H+ = H+
699     log_k    0
700 SURFACE_MASTER_SPECIES
701 Alo_b Alo_bO-1.5
702 Alo_c Alo_cO-0.75
703 Alo_e Alo_eO-0.5
704
705 Alp_a Alp_aO-1.25
706 Alp_b Alp_bO-1.5
707 Alp_c Alp_cO-0.75
708 Alp_d Alp_dO-1
709 Alp_e Alp_eO-0.5
710
711 SURFACE_SPECIES
712     # face (100)
713
714 Alo_bO-1.5 = Alo_bO-1.5
715 log_k 0
716 -cd_music 0 0 0
717
718 Alo_bO-1.5 + Na+ = Alo_bONa-0.5
719 log_k -0.096
720 -cd_music 0 0 1
721
722 Alo_bO-1.5 + H+ = Alo_bOH-0.5
723 -cd_music 1 0 0
724 log_k 20.6
725
726 Alo_bOH-0.5 + Na+ = Alo_bOHNa+0.5
727 log_k -0.096
728 -cd_music 0 0 1
729
730 Alo_bOH-0.5 + H+ = Alo_bOH2+0.5
731 -cd_music 1 0 0
732 log_k 8.16 #8.72
733
734 Alo_bOH2+0.5 + Cl- = Alo_bOH2Cl-0.5
735 log_k -0.176
736 -cd_music 0 0 -1
737
738 Alo_cO-0.75 = Alo_cO-0.75
739 log_k 0
740 -cd_music 0 0 0
741
742 Alo_cO-0.75 + Na+ = Alo_cONa+0.25
743 log_k -0.096
744 -cd_music 0 0 1

```


745
746 $\text{AlO}_c\text{O}-0.75 + \text{H}^+ = \text{AlO}_c\text{OH}+0.25$
747 $-\text{cd_music } 1 \ 0 \ 0$
748 $\log_k \ 10.32$
749
750 $\text{AlO}_c\text{OH}+0.25 + \text{Cl}^- = \text{AlO}_c\text{OHCl}-0.75$
751 $\log_k \ -0.176$
752 $-\text{cd_music } 0 \ 0 \ -1$
753
754 $\text{AlO}_c\text{OH}+0.25 + \text{H}^+ = \text{AlO}_c\text{OH}_2+1.25$
755 $-\text{cd_music } 1 \ 0 \ 0$
756 $\log_k \ -2.64 \ \#-1.56$
757
758
759 $\text{AlO}_c\text{OH}_2+1.25 + \text{Cl}^- = \text{AlO}_c\text{OH}_2\text{Cl}+0.25$
760 $\log_k \ -0.176$
761 $-\text{cd_music } 0 \ 0 \ -1$
762
763 $\text{AlO}_e\text{O}-0.5 = \text{AlO}_e\text{O}-0.5$
764 $\log_k \ 0$
765 $-\text{cd_music } 0 \ 0 \ 0$
766
767 $\text{AlO}_e\text{O}-0.5 + \text{Na}^+ = \text{AlO}_e\text{ONa}+0.5$
768 $\log_k \ -0.096$
769 $-\text{cd_music } 0 \ 0 \ 1$
770
771 $\text{AlO}_e\text{O}-0.5 + \text{H}^+ = \text{AlO}_e\text{OH}+0.5$
772 $-\text{cd_music } 1 \ 0 \ 0$
773 $\log_k \ 5.94$
774
775 $\text{AlO}_e\text{OH}+0.5 + \text{Cl}^- = \text{AlO}_e\text{OHCl}-0.5$
776 $\log_k \ -0.176$
777 $-\text{cd_music } 0 \ 0 \ -1$
778
779 $\text{AlO}_e\text{OH}+0.5 + \text{H}^+ = \text{AlO}_e\text{OH}_2+1.5$
780 $-\text{cd_music } 1 \ 0 \ 0$
781 $\log_k \ -9.84 \ \#-5.94$
782
783 $\text{AlO}_e\text{OH}_2+1.5 + \text{Cl}^- = \text{AlO}_e\text{OH}_2\text{Cl}+0.5$
784 $\log_k \ -0.176$
785 $-\text{cd_music } 0 \ 0 \ -1$
786
787 $\# \text{ face } (110)$
788
789
790 $\text{Alp}_a\text{O}-1.25 = \text{Alp}_a\text{O}-1.25$
791 $\log_k \ 0$
792 $-\text{cd_music } 0 \ 0 \ 0$
793
794 $\text{Alp}_a\text{O}-1.25 + \text{Na}^+ = \text{Alp}_a\text{ONa}-0.25$
795 $\log_k \ -0.096$
796 $-\text{cd_music } 0 \ 0 \ 1$
797
798 $\text{Alp}_a\text{O}-1.25 + \text{H}^+ = \text{Alp}_a\text{OH}-0.25$

799 -cd_music 1 0 0
800 log_k 12.97
801
802 $\text{Alp_aOH-0.25} + \text{Na}^+ = \text{Alp_aOHNa+0.75}$
803 log_k -0.096
804 -cd_music 0 0 1
805
806 $\text{Alp_aOH-0.25} + \text{H}^+ = \text{Alp_aOH2+0.75}$
807 -cd_music 1 0 0
808 log_k 0.12 #1.09
809
810 $\text{Alp_aOH2+0.75} + \text{Cl}^- = \text{Alp_aOH2Cl-0.25}$
811 log_k -0.176
812 -cd_music 0 0 -1
813
814 $\text{Alp_bO-1.5} = \text{Alp_bO-1.5}$
815 log_k 0
816 -cd_music 0 0 0
817
818 $\text{Alp_bO-1.5} + \text{Na}^+ = \text{Alp_bONa-0.5}$
819 log_k -0.096
820 -cd_music 0 0 1
821
822 $\text{Alp_bO-1.5} + \text{H}^+ = \text{Alp_bOH-0.5}$
823 -cd_music 1 0 0
824 log_k 21.22
825
826 $\text{Alp_bOH-0.5} + \text{Na}^+ = \text{Alp_bOHNa+0.5}$
827 log_k -0.096
828 -cd_music 0 0 1
829
830 $\text{Alp_bOH-0.5} + \text{H}^+ = \text{Alp_bOH2+0.5}$
831 -cd_music 1 0 0
832 log_k 9.16 #9.34
833
834 $\text{Alp_bOH2+0.5} + \text{Cl}^- = \text{Alp_bOH2Cl-0.5}$
835 log_k -0.176
836 -cd_music 0 0 -1
837
838 $\text{Alp_cO-0.75} = \text{Alp_cO-0.75}$
839 log_k 0
840 -cd_music 0 0 0
841
842 $\text{Alp_cO-0.75} + \text{Na}^+ = \text{Alp_cONa+0.25}$
843 log_k -0.096
844 -cd_music 0 0 1
845
846 $\text{Alp_cO-0.75} + \text{H}^+ = \text{Alp_cOH+0.25}$
847 -cd_music 1 0 0
848 log_k 10.45
849
850 $\text{Alp_cOH+0.25} + \text{Cl}^- = \text{Alp_cOHCl-0.75}$
851 log_k -0.176
852 -cd_music 0 0 -1

853
854 $\text{Alp_cOH}+0.25 + \text{H}^+ = \text{Alp_cOH}2+1.25$
855 $-\text{cd_music } 1 \ 0 \ 0$
856 $\log_k -1.90 \ \#-1.43$
857
858 $\text{Alp_cOH}+0.25 + \text{Cl}^- = \text{Alp_cOHCl}-0.75$
859 $\log_k -0.176$
860 $-\text{cd_music } 0 \ 0 \ -1$
861
862 $\text{Alp_dO}-1 = \text{Alp_dO}-1$
863 $\log_k 0$
864 $-\text{cd_music } 0 \ 0 \ 0$
865
866 $\text{Alp_dO}-1 + \text{Na}^+ = \text{Alp_dONa}$
867 $\log_k -0.096$
868 $-\text{cd_music } 0 \ 0 \ 1$
869
870 $\text{Alp_dO}-1 + \text{H}^+ = \text{Alp_dOH}$
871 $-\text{cd_music } 1 \ 0 \ 0$
872 $\log_k 13.86$
873
874 $\text{Alp_dOH} + \text{H}^+ = \text{Alp_dOH}2+1$
875 $-\text{cd_music } 1 \ 0 \ 0$
876 $\log_k 0.29 \ \#1.98$
877
878 $\text{Alp_dOH}2+1 + \text{Cl}^- = \text{Alp_dOH}2\text{Cl}$
879 $\log_k -0.176$
880 $-\text{cd_music } 0 \ 0 \ -1$
881
882 $\text{Alp_eO}-0.5 = \text{Alp_eO}-0.5$
883 $\log_k 0$
884 $-\text{cd_music } 0 \ 0 \ 0$
885
886 $\text{Alp_eO}-0.5 + \text{Na}^+ = \text{Alp_eONa}+0.5$
887 $\log_k -0.096$
888 $-\text{cd_music } 0 \ 0 \ 1$
889
890 $\text{Alp_eO}-0.5 + \text{H}^+ = \text{Alp_eOH}+0.5$
891 $-\text{cd_music } 1 \ 0 \ 0$
892 $\log_k 4.75$
893
894 $\text{Alp_eOH}+0.5 + \text{Cl}^- = \text{Alp_eOHCl}-0.5$
895 $\log_k -0.176$
896 $-\text{cd_music } 0 \ 0 \ -1$
897
898 $\text{Alp_eOH}+0.5 + \text{H}^+ = \text{Alp_eOH}2+1.5$
899 $-\text{cd_music } 1 \ 0 \ 0$
900 $\log_k -8.60 \ \#-7.13$
901
902 $\text{Alp_eOH}2+1.5 + \text{Cl}^- = \text{Alp_eOH}2\text{Cl}+0.5$
903 $\log_k -0.176$
904 $-\text{cd_music } 0 \ 0 \ -1$
905
906

```

907 USER_GRAPH
908 chart_title "charge de surface de l'alumine"
909   -headings pH Alo_bOH-0.5 Alo_bOH2+0.5 Alo_cO-0.75 Alo_cOH+0.25 Alo_eO-
910   0.5 Alo_eOH+0.5 charge_Alo Alp_aOH-0.25 Alp_aOH2+0.75 Alp_bOH-0.5
911   Alp_bOH2+0.5 Alp_cO-0.75 Alp_cOH+0.25 Alp_dOH Alp_eO-0.5 Alp_eOH+0.5
912   charge_Alp psil Na_ads Cl_ads Alo_pO-1.5 Alo_pOH-0.5
913   -connect_simulations true
914   -initial_solutions false
915   -axis_titles pH sigma
916   -axis_scale x_axis 2 12 2 1 # minimum 0, maximum 350, major tics at 50,
917   minor tics at 25
918   # -axis_scale y_axis -8 -3 1
919   -start
920   10 graph_x -la("H+")
921   30 graph_sy mol("Alo_bOH-0.5"), mol("Alo_bOH2+0.5")
922   40 graph_sy mol("Alo_cO-0.75"), mol("Alo_cOH+0.25")
923   60 graph_sy mol("Alo_eO-0.5"), mol("Alo_eOH+0.5")
924   70 graph_y EDL("Sigma","Alo")
925   120 graph_sy mol("Alp_aOH-0.25"), mol("Alp_aOH2+0.75")
926   130 graph_sy mol("Alp_bOH-0.5"), mol("Alp_bOH2+0.5")
927   140 graph_sy mol("Alp_cO-0.75"), mol("Alp_cOH+0.25")
928   150 graph_sy mol("Alp_dOH")
929   160 graph_sy mol("Alp_eO-0.5"), mol("Alp_eOH+0.5")
930   170 graph_y EDL("Sigma","Alp")
931   200 graph_y 0.32*EDL("psil","Alp")+0.08*EDL("psil","Alo")
932   +0.6*EDL("psil","Alpo")
933   210 graph_y 0.8*surf("Na","Alp")+0.2*surf("Na","Alo")
934   220 graph_y 0.8*surf("Cl","Alp")+0.2*surf("Cl","Alo")
935   230 graph_y EDL("psil","Alpo")
936   240 graph_sy mol("Alo_pO-1.5"), mol("Alo_pOH-0.5")
937   -end
938
939 SOLUTION 1
940   Na 100 charge; Cl 100
941 SURFACE 1
942   -sites_units density # site concentration in sites/nm^2
943   Alo_b 0 40 1.0 # 2.17 40 2.0
944   Alo_c 0 # 1.09
945   Alo_e 0 # 1.09
946
947   Alp_a 0 160 1.0 #1.49
948   Alp_b 0 #1.49
949   Alp_c 2.99 # 2.99
950   Alp_d 0.25 # 1.49
951   Alp_e 1.49 # 1.49
952
953   # Alo_b moyen sur la particule : 2 site/nm2
954
955   -capacitance 1.39 5
956   -equilibrate 1
957   -cd_music
958
959
960 EQUILIBRIUM_PHASES;Fix_H+ -2.8 HCl1 END

```


962

963 **References**

964

- 965 1. Corral Valero, M., Prelot, B. & Lefèvre, G. MUSIC Speciation of γ -Al₂O₃ at the Solid Liquid
966 Interface: How DFT Calculations Can Help with Amorphous and Poorly Crystalline Materials.
967 *Langmuir* **35**, 12986–12992 (2019).

968